2D+1 degree of freedom equivalent circuit model for LiNbO3/metal/LiNbO3 bimorph bending cantilever

Giacomo Clementi, Mario Costanza, Merieme Ouhabaz, Ausrine Bartasyte, Bernard Dulmet, Samuel Margueron

2D+1 Degree of Freedom Equivalent Circuit Model for $LiNbO_3$/metal/$LiNbO_3$ Bimorph Bending Cantilever

Giacomo Clementi, Mario Costanza, Merieme Ouhabaz, Ausrine Bartasyte, Bernard Dulmet, Samuel Margueron*

FEMTO-ST Institute, University of Franche-Comté, CNRS (UMR 6174), ENSMM, 26 rue de l'Epitaphe, Besançon, 25030, France

Abstract

In this paper, we extend the single degree of freedom (1DOF) model to a lumped circuit model derived analytically with three degrees of freedom (2D+1DOFs) for modelling the mechanical-to-electrical conversion by a serial bimorph piezoelectric cantilever. The model is based on a minimal finite element analysis interpolation of the beam bending with two mechanical nodes and four symmetrical electrical nodes. The model satisfies Hamilton's principle, Euler-Bernoulli kinematic assumptions and constitutive piezoelectric equations. The 2D+1DOFs are the transverse displacement, the rotation at the tip end, and the voltage output. The DOFs result from the application of three external actions: the vertical tip force, the tip torque and the net electrical charge on the electrodes. The dynamic balance of the bimorph is described by three electromechanical coupled equations that are equivalently rendered by two mutually coupled electronic resonant lumped circuits driven by the mechanical DOFs, and an output circuit involving the charge and the external load. As compared to 1DOF equivalent circuit, this model introduces analytically and parametrically the geometry of the beam and its properties for transient and frequency-domain analysis using computer-aided electronics software. The results of the model are compared to the simulations done by using commercial finite element modelling software and the experimental measurements of a symmetric $LiNbO_3$/stainless steel/$LiNbO_3$ serial bimorph beam resonating at 35.7 Hz. Monte Carlo simulations including uncertainty on geometrical parameters show less than 2% of uncertainty on open circuit voltage and resonance frequency. Our lead-free bimorph shows an electromechanical coupling of k^2 = 5.2 %.

Keywords: Piezoelectric Bimorph, Energy Harvesting, Finite element Analysis, $LiNbO_3$ on Metal, Equivalent Circuit Modeling

1. Introduction

There is a drastically increasing number of communicating sensors with the expansion of Industry 4.0, the Internet of Things (IoT), the Internet of Humans/Health (IoH), smart cities or autonomous vehicles [1, 2, 3]. It is becoming necessary to simplify energy supply while offering sustainable solutions. Energy micro-source based on piezoelectric conversion is an appealing solution for micro-electric energy supply [4, 5] in case of shocks, vibrations and movement conversion and it can be used for indoor (industrial machinery, cars) and outdoor (human body movements, wearables, bridges) [6, 7] applications.

* Corresponding author. Tel.: +33-381-402-926; fax: +33-381-885-714.
E-mail address: samuel.margueron@femto-st.fr.

Meanwhile, the most common mechanical structures used for this purpose are resonant cantilevered beams based on lead containing piezoelectric materials (PZT, PMT-PT). In this case, the piezoelectric material has the capability of converting flexural deformation into an electric voltage [8]. Piezoelectric harvesters can generate suitable voltage levels (typically from 1 V to 20 V, depending on the volume of the active layer), and high-power density (> 300 $\mu W/cm^3$) for IoT sensors. However, to meet RoHS and European REACH regulations, the material chosen in this work is lead-free $LiNbO_3$, which, as recently shown, presents equivalent electromechanical properties to commonly used PZT ceramics [9, 10]. This piezoelectric material is available in the form of cheap large single crystals (up to 150 mm diameter). Moreover, we have shown that a simple unimorph cantilever presented a high electromechanical coupling (k^2) for vibrational energy harvesting applications [11], opening new opportunities for lead-free micro-energy sources adapted to daily basis user electronics autonomous solutions [12]. Recently, $LiNbO_3$ has been also used to power IoT nodes, either with commercial radiofrequency modules [13] or Bluetooth [14]. Nevertheless, these papers evaluated $LiNbO_3$-on-silicon unimorphs. Bimorph structures are expected to double the performances. Recently, some authors have also evaluated $LiNbO_3$ bimorph structures with opposite polarization directions in two piezoelectric layers for actuation and energy harvesting [15,16], but in the form of thick single crystals and no optimization of the electromechanical coupling has been performed.

Concerning the modelling of piezoelectric flexible energy harvesters (or micro-electric generators), an early analysis was based on inertial electromechanical transducers [17]. The spring (k) – mass (m) – damper (ζ) system of relative motion z(t) was moving out of phase with the generator housing under an input motion y(t). Assuming that the damping was due to the electrical conversion, the maximum power output at resonant frequency, ω, was proposed to be $P = m \zeta \omega^3 z_{(max)}^2$. Roundy and al. [18] extended this model by replacing the electrical conversion damping, ζ', by a lumped circuit made of a transformer as in Mason's circuits [19]. In terms of unidirectional motion, the 1DOF system introduced a bridge between the mechanical and the electrical circuit interface. Moreover, the authors proposed analytical expressions for evaluating spring (k) – mass (m) – damper (ζ) in the case of a bimorph bending cantilever. Meanwhile, modelling of a piezoelectric cantilever beam introducing continuous media with piezoelectric elements was proposed by Tiersten [20], Tanaka [21], and duToit et al. [22]. The model is based on Hamilton's principle and Bernoulli's approximation to analyse the response of a piezoelectric energy harvester. However, the reported works are missing an electrical equivalent circuit model, and its application with a suitable electronic interface. In fact, the analysis of literature shows a loose correspondence between electrical and mechanical engineering for modelling either the mechanical system [23,24], or the electrical interfaces [25,26,27,28].

In this paper, we present an extension of 1DOF model based on Hamilton's principle applied on a bimorph piezoelectric beam. The model is presented in part 2.1 and Supplementary Material. Three coupled equations with two mechanical degrees of freedom, and one electrical port are used to model our harvester. One of the originalities of this paper is to present a lumped equivalent electronic circuit of the coupled equations mainly based on two resonant circuits and coupling loops. In our model, he approximated linear theory of piezoelectricity was employed along with the hypothesis of no free charges and body forces. The circuit is solved with standard computer-aided electronics software in part 2.2. In part 3.1, we describe the preparation of our samples and the determination of the parameters of the model. The results of our model are computed in transient and frequency-domain simulations in part 3.2 with the experimental parameters. For the first time, the bimorph cantilevers based on $LiNbO_3$ and stainless steel were fabricated and their performance in terms of vibrational energy harvesting were characterized. The experimental and modelling results on voltage output and

resonant frequency were compared in part 3.3. Moreover, we provide a Monte Carlo simulation on the uncertainty of geometrical parameters.

2. Theoretical Considerations

2.1 Electromechanical Equation of the bimorph

Assuming that our bimorph cantilever is conservative and elastic, the electro-mechanical problem is a lumped transformation, which consists of transforming external work into an oscillating structure converting kinetic energy to potential energy. The multi-layer is composed of piezoelectric and non-piezoelectric layers that should satisfy Hamilton's principle:

$$\delta \int_{t1}^{t2} \boldsymbol{L} dt + \delta \int_{t1}^{t2} \boldsymbol{\mathcal{W}} dt = 0, \quad (1)$$

Where $\boldsymbol{\delta \mathcal{W}}$ is the virtual work of external forces applied to the surface of the body and $\boldsymbol{L}$ – the Lagrangian of the system. The virtual work of the force (per unit area), $\boldsymbol{F}$, under an infinitesimal displacement, δu_k, and a charge, σ, under infinitesimal variation of potential, $\delta\varphi$, (in the piezoelectric layers) are given by the surface integration:

$$\boldsymbol{\delta \mathcal{W}} = \int_A F_k \delta u_k - \sigma \delta \varphi dA. \quad (2)$$

While the Lagrange can be written as:

$$\boldsymbol{L} = \int_V \frac{1}{2} \rho_0 \dot{u}_j \dot{u}_j - \boldsymbol{H_e}(S_{kl}, E_k) dV, \quad (3)$$

Where we recognize the kinetic energy, $\boldsymbol{\mathcal{T}}$, function of the initial mass density, ρ_0, and square of the speed of particles, $\dot{u}_j$, and $\boldsymbol{H_e = U - ED}$ - the electrical enthalpy per unit volume for the piezoelectric layers. The energy reduces to $\boldsymbol{H_e \equiv U}$ in the metal part. In our model, the approximated linear theory of piezoelectricity was employed along with hypothesis of no free charges and body forces. The derivation for our case study is described in Supplementary Material A & B.

The geometry of the serial bimorph is depicted in Figure 1. The piezoelectric bimorph is composed of two symmetrical $LiNbO_3$ piezoelectric layers and thickness, h_p, and a central core made of stainless-steel layer with thickness $2h_m$. The origin of the bimorph is the neutral plane ($z = 0$), of the total thickness $2h = 2h_p + 2h_m$, width, b, and length, L. The beam is supposed to be clamped in $x = 0$ and free in $x = L$ which are the mechanical nodes of our system. Moreover, the serial bimorph is composed of two piezoelectric layers with opposite polarization directions. The three electrical nodes of the circuit are constrained as follows: we arbitrarily set the potential to zero in the core metal ($\varphi_{hm} = \varphi_{-hm} = 0$) and we impose antisymmetric potential on the top and bottom electrode $\varphi_h = -\varphi_{-h}$ by applying symmetry considerations. The potential is assumed to be constant along the beam due to the metal layers adjacent to the major surfaces of the piezoelectric layers. From the static equilibrium, the virtual work of infinitesimal displacements applied on the beam takes the simple form:

$$\delta \boldsymbol{\Phi} = F_z^L \delta w_L + M_y^L \delta w_L' - 2Q_h \, \delta(\varphi_h), \quad (4)$$

Where F_z^L, M_y^L are the force and the momentum exerted at the tip of the beam, respectively, $-Q_h$ - the charge on the top surface electrodes, whereas, the three degrees of freedom are w_L, w_L' - the transverse displacements and its rotation in x = L, and $2\varphi_h$ - the potential between the top and bottom

surface. One can note that there are opposed force and momentum in $x = 0$, but they do not contribute to the work, due to the clamped conditions ($w_0 = 0$ and $w'_0 = 0$).

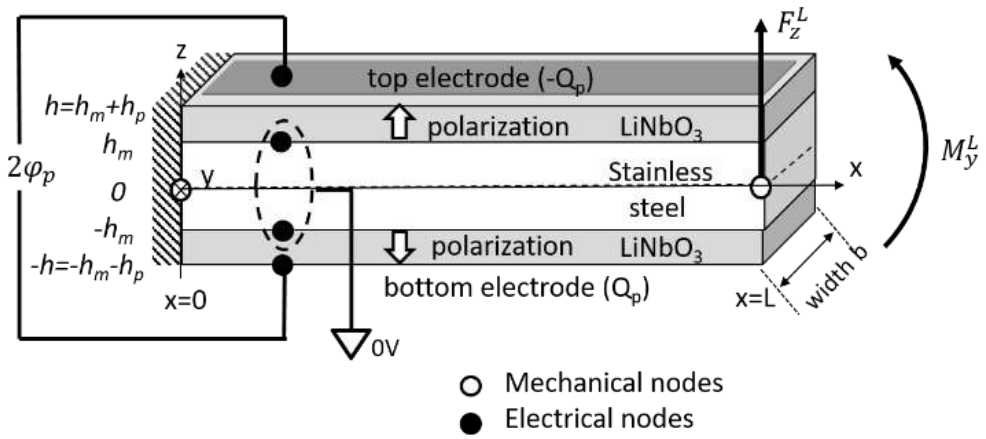

Figure 1: 2D+1 model of $LiNbO_3$ bimorph in series configuration. The mechanical beam is defined at the two nodes: clamped in $x = 0$ and free in $x = L$. The electrical potential is defined by four symmetrical nodes with the central ones set at zero potential.

In Supplementary Material C & D, we have derived the expression of the kinetic energy and electrical enthalpy terms of Equation 3 using Bernoulli's approximation. The results lead to a differential equation of the three degrees of freedom, w_L, w'_L and $2\varphi_h$. An approximated solution of this linear differential equation is proposed using Galerkin's Finite Element Method. We have defined 2 mechanical nodes (in $x = 0$ and $x = L$) and 4 symmetrical electrical nodes (in $z = -h$, $z = -h_m$, $z = +h_m$ and $z = h$). The beam bending and its rotation, w and w', are approximated by trial cubic splines in x, whereas, the potential, φ_h, is supposed to be linear along the thickness, z, of the piezoelectric layers. The discretization of the equation as a function of the generalized-force vector components exerted on the beam ($-Q_h$, C_y^L, F_z^L) and the variables ($2\varphi_h, w_L, w'_L$) leads to a 3x 3 dynamic equation:

$$\left(\begin{bmatrix} K_{11} & 0 & K_{13} \\ 0 & K_{22} & K_{23} \\ K_{31} & K_{32} & K_{33} \end{bmatrix} - \omega^2 \begin{bmatrix} 0 & 0 & 0 \\ 0 & M_{22} & M_{23} \\ M_{31} & M_{32} & M_{33} \end{bmatrix}\right) \begin{Bmatrix} \varphi_h \\ w_L \\ w'_L \end{Bmatrix} = \begin{Bmatrix} -2Q_h \\ F_z^L \\ M_y^L \end{Bmatrix} \quad (5)$$

Where ω is the excitation frequency, and the $\boldsymbol{K}$ and $\boldsymbol{M}$ are the stiffness and mass matrices, respectively (defined in Supplementary Material). The system of the Equation 5 gives the voltage- or charge-driven frequency response by setting $M_y^L = 0$ and $F_y^L = 0$. In the case of vibration-driven harvester, one has to add the vertical component of the driving acceleration, Γ_z. Setting $F_z^L = M_{22}\Gamma_z$ and neglecting the Coriolis force if the frame does not rotate, one can solve the problem for a vibrational harvester.

2.2 Equivalent circuit modelling

One very important aspect of this work is to give an equivalent electrical circuit of the variables defined in Equation 5. Details of the calculations are given in Supplementary Material E. We start by defining three currents expressed in harmonic regime as:

$$\begin{aligned} I_h &= 2j\omega Q_h, \\ I_p &= j\omega K_{13} w'_L, \text{ and} \\ I_w &= j\omega \alpha w_L, \end{aligned} \tag{6}$$

With $\alpha = K_{13}/\mathrm{L}$. Replacement of the current (defined by the Equation 6) in the Equation 3 gives three coupled equations as a function of I_h, I_p and I_w:

$$\begin{aligned} \varphi_h &= \frac{I_h + I_p}{j\omega C_0} \\ E_F &= \frac{(1-\omega^2 L_1 C_1)}{j\omega C_1} I_w + \frac{(1-\omega^2 L_c C_c)}{j\omega C_c} I_p \\ E_T &= \varphi_h + \frac{(1-\omega^2 L_c C_c)}{j\omega C_c} I_w + \frac{(1-\omega^2 L_2 C_2)}{j\omega C_2} I_p \end{aligned} \tag{7}$$

With $C_0 = -K_{11}$, $L_1 = \frac{M_{22}}{\alpha^2}$, $C_1 = \frac{\alpha^2}{K_{22}}$, $L_c = \frac{M_{23}}{\alpha K_{13}}$, $C_c = \frac{\alpha K_{13}}{K_{23}}$, $L_2 = \frac{M_{33}}{{K_{13}}^2}$, $C_2 = \frac{{K_{13}}^2}{K_{33}}$, $E_F = F_z^L/\alpha$, where $\alpha = K_{13}/L$, and $E_T = -M_y^L/K_{13}$. The first equation is related to the first loop of potential, φ_h, and it represents the output voltage of the piezoelectric bimorph in terms of the two currents (I_h, I_p). In the second equation, we have to transform F_z^L into a voltage ($E_\mathrm{F} = \frac{K_{13}}{\mathrm{L}} F_z^L$). This represents the external loop, where the L_1C_1 term appears along with the L_cC_c which represents a cross-coupling component to the I_p current and it is computed in a separate loop as the voltage E_Q on the "Q" node. Using the same reasoning, one can obtain the expressions for the third equation, where we define another voltage source as E_T. Here, the current I_w is also cross-coupled through the voltage E_N on the node "N" in a secondary loop with current I_w. Eventually, in the equivalent circuit some resistors as r_1, r_2 and metal are added, which are purely dissipative terms to take into account the losses of the contacts and the material. R_l is the load of the harvester needed to evaluate the power harvested. Finally, these equations were implemented in terms of the equivalent circuit parameters as depicted in Figure 2.

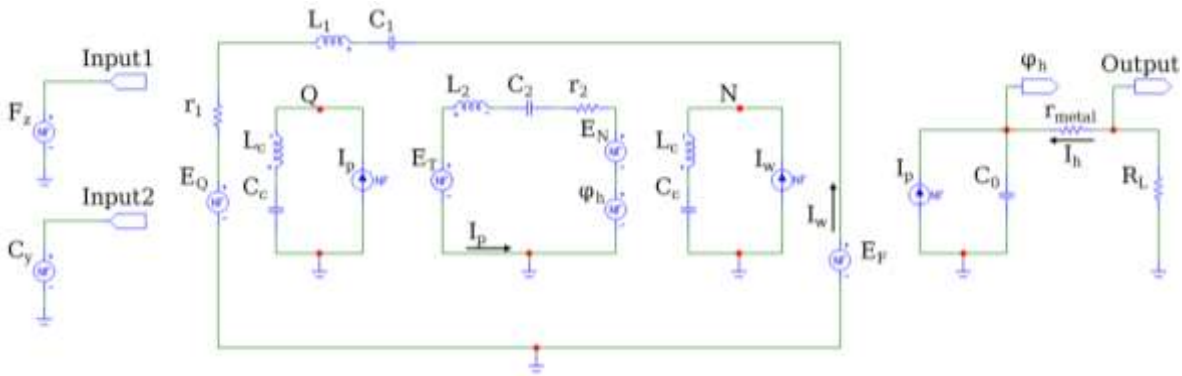

Figure 2: Equivalent circuit implemented for simulation in computer-aided electronics software.

3 Validation of the model

3.1 Fabrication and characterization of $LiNbO_3$/SS/$LiNbO_3$ bimorph

The bimorph was fabricated by means of wafer-on-wafer technology, using poled 128°-$LiNbO_3$ single wafers bonded in opposite polarity on both faces of a stainless steel (SS) shim of h_m = 60 µm (serial configuration). The surfaces of $LiNbO_3$ wafers and stainless steel were coated with 100 nm of gold (Au) by sputtering and compressed to bond at room temperature with EVG bonder. The two piezoelectric layers were subsequently polished down until the required thickness (h_p = 55 ± 5 µm). Finally, the multi-layer wafer was mechanically diced in order to obtain rectangular cantilevers with the width parallel to the X-axis of $LiNbO_3$. Electrodes of Cr/Au (50 nm / 150 nm) were sputtered through a stencil mask. The final dimensions of the cantilever were L = 70 mm, b = 10 mm and h = 170 µm. Above-measured thicknesses may present an uncertainty of up to 10% along the beam. Table 1 summarizes physical parameters of $LiNbO_3$/SS/$LiNbO_3$ bimorph structure, used in the following calculations/simulations. The effective dielectric constant, $\varepsilon_{33}^{T}{}'$ and piezoelectric coefficient, d'_{31}, of $LiNbO_3$ corresponding to the (YXlt)/128°/90° $LiNbO_3$ rotated tensor values are given in the Table 1 [29]. Full details about $LiNbO_3$ properties are discussed in Ref [30, 31]. In this work we systematically used the nomenclature of effective piezoelectric coefficient d'_{31} even though the proper definition for (YXlt)/128°/90° $LiNbO_3$ would be effective d'_{23}.

Table 1. Physical parameters of the bimorph $LiNbO_3$/SS/$LiNbO_3$ structure in the series configuration.

Parameter	Value	Units
d'_{31}	27	$pC.N^{-1}$
$\varepsilon_{33}^{T}{}'$	50.5	-
F_z	0.05	G_{peak}
h_i	50	µm
h_p	55	µm
L	70	mm

ρ_i	7850	kg.m^{-3}
ρ_p	4650	kg.m^{-3}
Q	90	-
$s_{i,11}$	5.72e-12	Pa^{-1}
$s_{p,11}$	6.91e-12	Pa^{-1}
b	10	mm

The characterization setup is presented in Figure 3. The cantilever was clamped with two isolated aluminum plates on the shaker. The plates were wired for measurements. For the electromechanical characterization, we used a spectrum analyzer (KEYSIGHT E5061B), in order to estimate the capacitance, electromechanical coupling and quality factor of the piezoelectric harvester. The clamped capacitance of the specimen, measured out of resonance at 1 kHz, was C_0 = 1.35 nF, while the quality factor in resonance (~35.4 Hz) was Q = 93 and the electromechanical coupling k^2 = 5.2 %. These results are comparable to our previous works on unimorph $LiNbO_3$/silicon cantilevers [11]. It is important to note that the electromechanical coupling factor of $LiNbO_3$/SS/$LiNbO_3$ structure was higher by a factor of two than that of unimorph $LiNbO_3$/Si structure (k^2 = 2.8 %). This denotes the high quality of the bimorph on stainless steel. The damping of the structure was added by introducing a resistor in the electrical circuit and the experimentally measured quality factor Q was ~ 90 at the resonance.

For the vibrational harvesting measurements, the device was connected to a full-bridge rectification circuit using four diodes (FJH1100), to convert the alternative electric potential of the harvester in DC signal, and a smoothing capacitor (C_r = 1 μF). The excitation signal was generated by a National Instrument acquisition card (NI USB-6341) in the form of sinusoidal excitation to drive a power amplifier (LDS PA100E) and an electrodynamic LDS shaker. A laser probe (KEYENCE LB-12) was focused on the tip of the cantilever to measure the displacement during the tests with an oscilloscope (LECROY LT344). As for measurements without rectifiers, the measurements were done using an oscilloscope (Rohde & Schwartz RTB2004) with a 10 MΩ probe.

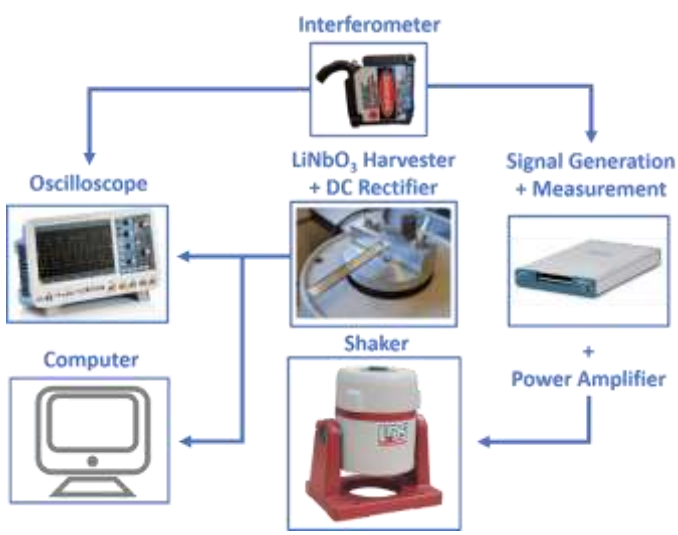

Figure 3: Experimental setup used for vibrational harvester characterization and FEA validation.

3.2 Transient and time domain simulations

The implementation of the equivalent circuit was carried out by using SPICE with the software Micro-Cap 12, where both time domain and transient simulations were investigated. We can simulate the piezoelectric device with such equivalent circuit starting directly from the geometrical and material parameters, which are translated from the theoretical model to the final expression in the circuit. Considering the physical parameters of the harvester, listed in Table 1, we have calculated the parameters of the model given in the Supplementary Material. Table 2 gives the numerical values for the discrete components in the equivalent circuit of Figure 2.

Table 2. Numerical parameters of the equivalent electrical circuit.

Parameter	Value	Units
C_0	8.70e-9	F
C_1	25.03e-3	F
C_2	140.53e-12	F
C_c	2.17e-6	F
L_1	337.79e-6	µm
L_2	4.60e3	mm
L_c	1.095	$kg.m^{-3}$
r_1	643.47e-6	Ohm
r_2	31.79e3	Ohm
metal	1 (arbitrary)	Ohm

One of the advantages of our approach is to implement the equations of our model in transient analysis. Dealing with a single node provides lighter calculations to solve but still accurate results, hence we can obtain information regarding the main potential, φ_h, displacement, w, and rotation ,w', of the piezoelectric bimorph. Moreover, using such equivalent circuit unites both finite element modelling approach and lumped model simulations, giving the possibility of connecting any electronic circuitry to the modelled energy harvester. Hence, the simulations carried out implied both a simple connection to a resistive load, R_l, and solved in time domain (no non-linear element), in order to analyze the peak voltage and expected instantaneous power output of the harvester. In the second part, a rectifying diode bridge with a storage-filtering capacitor is introduced in the output and solved in transient analysis. The latter is especially important because we can precisely assess the rectified power output that can be used directly to power up an IoT node, or design a suitable electronic configuration for power management purposes.

In Figure 4a a comparison of the output variables in the frequency domain is presented, when the piezoelectric bender is excited with a peak base acceleration of 0.05 g (g = 9.81 $m.s^{-2}$). The resonance frequency for the bending mode is at 36.535 Hz, a voltage output of 10.23 V is reached for 20 MΩ load, with a peak displacement of 803 µm and a maximal rotation of 0.0146 rad. In Figure 4b we present the transient analysis of the bimorph excited at resonance frequency. The voltage output of the resistive load reaches the maximum value after 3 s, and the same is for rotation and displacement. In Figure 4c and 4d, we implement a frequency domain and transient simulation with a diode bridge

rectification circuit, consists of four diodes and followed by a smoothing capacitor. The resonance frequency is the same as previously, but the electronic interface introduces an additional damping on the piezoelectric structure observed by an increase of the width of the resonant peak and reduces the measured output voltage. The peak voltage drops to 5.86 V, the displacement – to 535 μm, and the rotation changes to 0.097 rad. The voltage requires 30 s to completely charge the capacitor and store the electric energy provided by the piezoelectric harvester.

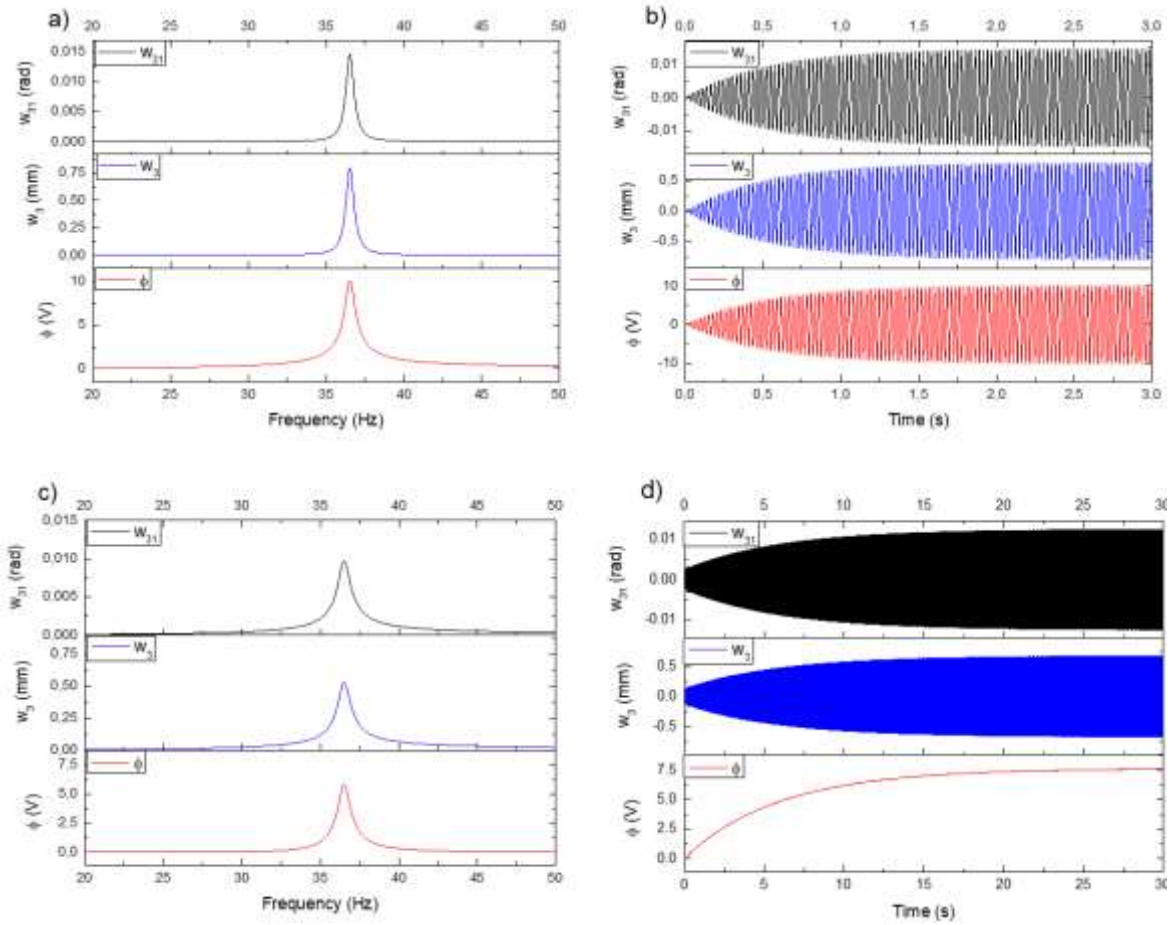

Figure 4: Frequency domain simulations and transient analysis of displacement, W_3, rotation, W_{31}, and output voltage, ϕ, for $LiNbO_3$ bimorph harvesters with a-b) resistive load and c-d) bridge rectifier and 1 μF storage capacitor. The transient analysis for the diode bridge is presented on a 10X longer scale.

3.3 Cross-check of the model

In Figure 5a, the peak voltage responses experimentally measured with the resistive load or the rectified voltage circuit are reported. The peak voltages are at 10.156 V and 6.819 V, respectively. We have obtained a good agreement between the peak voltage predicted earlier in the RMS simulations (Figure 3a), while observing a small discrepancy in terms of resonance frequency (35.7 Hz measured experimentally and 36.535 Hz predicted theoretically). For the rectified voltage peak the magnitude of the signal is in good agreement with the predictions of finite element analysis, even though the curve profile tend to bend on the left compared to the RMS counterpart. This effect may be due to the damping effect provided by the diode bridge used to measure the voltage, which is introducing non-linearity on the system[32,33], or introduced by capacitive or inductive terms [34]. In Figure 5b the rectified power output is presented. The test was carried out at resonance frequency while the rectified voltage was measured through the electronic variable resistive load. The maximum power measured was 3.67 µW for a load of 8 MΩ, resulting in a normalized power density of 209.7 $\mu W.cm^{-2}.g^{-2}$. The simulations are in good agreement with the results, even though they seem to underestimate the power output of the harvester. In this case the clamping force applied directly on the piezoelectric harvester can introduce some uncertainties, having an impact on the quality factor and the electromechanical coupling of the structure. On the other hand, the high resistive matching load is partially due to the fact that the clamped capacitance is only 1.35 nF for a relatively low resonance frequency of 35.4 Hz. Nevertheless, the value of the clamped capacitance can be further improved by using thinner piezoelectric layers, or connecting them in parallel rather than in the series.

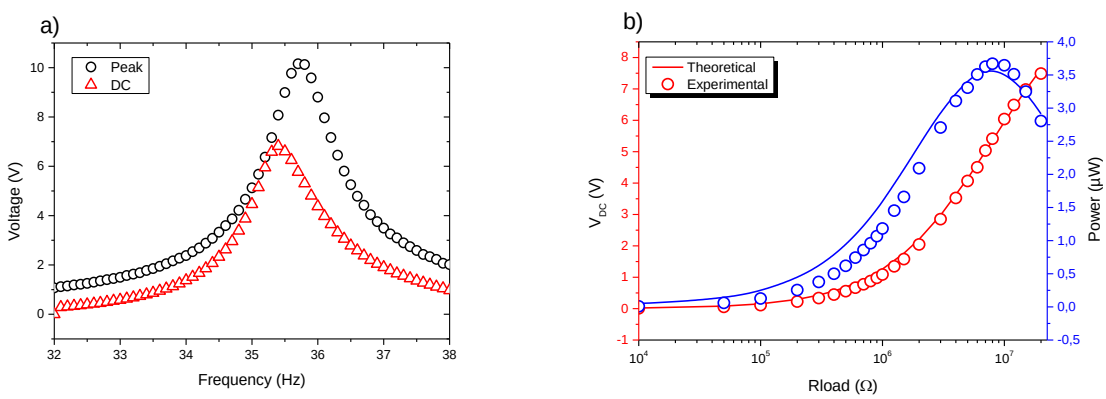

Figure 5: Comparison of experimental results (symbols) and simulations (lines) for bimorph $LiNbO_3/SS/LiNbO_3$ structure in the series configuration: a) voltage peak (open) and rectified voltage as a function of the frequency; b) rectified power and voltage, measured at resonance frequency, as a function of R_{load}.

For the model validation, we have compared the simulations previously done with our model and the experimental results as well as with COMSOL Multiphysics. Simulations were carried out considering the voltage peak value with the resistive load case of study; thus, no diode was connected to the piezoelectric harvester. In Figure 6, both COMSOL Multiphysics and equivalent circuit model were determined from beam dimensions of Table 1. The voltage peak and resonant frequency present similar values and a good agreement with the experimental results on the voltage peak values (±

0.16%) and the resonant frequency (± 2 %). Next, we have performed a sensitivity analysis with Monte Carlo simulations varying by 10 % (corresponding to the experimental precision in piezoelectric layer thickness) the value of the piezoelectric layer thickness, h_p, in the equivalent circuit. The voltage and the frequency response as a function of the value of h_p present Gaussian-type distribution center around the initial guess (Figure 6). This analysis shows that the discrepancy with the experimental values originates from uncertainty on the physical dimensions of the harvester such as the thickness, h_p. An optimization could improve the determination of the real parameters of the model of Table 1. Meanwhile, the main uncertainty remains the symmetry of the harvester that is not included in our equivalent circuit model.

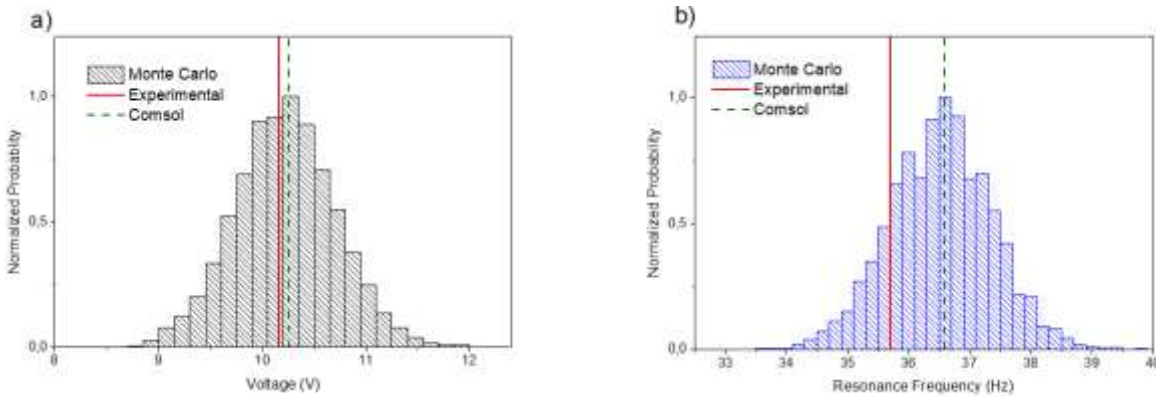

Figure 6: Monte Carlo simulations for a) peak voltage output and b) bending resonance frequency.

4 Conclusion

We have implemented an extended equivalent circuit modelling to predict and analyze the behavior of vibrational energy harvesters, based on bimorph cantilevers. The original theoretical framework based on finite element analysis can be applied not only to $LiNbO_3$ harvesters but in general to any other piezoelectric material. The presented model can be easily converted into an equivalent circuit and be used to perform transient and frequency domain simulations. This approach represents a fast implementation and accurate results for the first resonant mode. Furthermore, perfectly matching theoretical predictions for higher order modes can be obtained by increasing the number of nodes in the finite element model. Moreover, such formalism is versatile, and it can be applied to any kind of electromechanical problem, and especially for sensors and actuator systems.

$LiNbO_3$ represents an alternative to lead-based materials for harvesting and sensing applications, but until now only structures with a single piezoelectric layer were investigated. It was demonstrated that $LiNbO_3$ based harvesters can be a competitive solution with state-of-art energy harvesters as already demonstrated by unimorph $LiNbO_3$/Si[11] and $LiNbO_3$/brass structures[35], showing comparable performances to that of PZT. In this work we have investigated the possibility of using $LiNbO_3$ in bimorph configuration on stainless steel. The employed microfabrication technique is an upgrade compared to the technology used to obtain similar devices on silicon, in terms of cost and integration difficulty. Lower resonance frequencies (f_0 = 35.7 Hz) were attained for bimorph cantilever based on $LiNbO_3$ although the normalized power density (209.7 $\mu W.cm^{-2}.g^{-2}$) was lower than that of unimorph $LiNbO_3$/brass canilever operating at 66 Hz[35]. At the same time the coupling of the structure (k^2 =

5.2 %) has increased by a factor of two in comparison to our previous results on unimorph $LiNbO_3$/Si structure. The simulations, done by using our model, are in good agreement with the experimental results. Further structural optimization will be done to attain higher power density and the lifetime and robustness of the $LiNbO_3$/metal harvesters is under study.

Acknowledgements

The authors want to thank the financial supports of Bonus Quality Recherche program of ENSMM, MIMENTO from the French Renatech Network, EIPHI Graduate School contract ANR-17-EURE-0002, Itinéraire Chercheur Entrepreneur of Région Bourgogne Franche-Comté and H2020 MSCA-ITN Enhance project grant agreement No 722496.

References

[1] Raj, A., & Steingart, D. (2018). Review—Power Sources for the Internet of Things. Journal of The Electrochemical Society, 165(8), B3130.
[2] Zeadally, S., Shaikh, F. K., Talpur, A., & Sheng, Q. Z. (2020). Design architectures for energy harvesting in the Internet of Things. Renewable and Sustainable Energy Reviews, 128, 109901.
[3] Kiziroglou, M. E., & Yeatman, E. M. (2012). Materials and techniques for energy harvesting. Functional Materials for Sustainable Energy Applications, Woodhead Publishing Series in Energy 2021, pages 541–572.
[4] Pozo, B., Garate, J. I., Araujo, J. Á., & Ferreiro, S. (2019). Energy harvesting technologies and equivalent electronic structural models - review. Electronics (Switzerland), 8 (5), 1–31.
[5] Bowen, C. R., Kim, H. A., Weaver, P. M., & Dunn, S. (2014). Piezoelectric and ferroelectric materials and structures for energy harvesting applications. Energy and Environmental Science, 7(1), 25–44.
[6] Neri, I., Travasso, F., Mincigrucci, R., Vocca, H., Orfei, F., & Gammaitoni, L. (2012). A real vibration database for kinetic energy harvesting application. Journal of Intelligent Material Systems and Structures, 23(18), 2095–2101.
[7] Rantz, R., & Roundy, S. (2016). Characterization of real-world vibration sources with a view toward optimal energy harvesting architectures. Proceedings of the SPIE, Industrial and Commercial Applications of Smart Structures Technologies, Volume 9801, id. 98010P, 16.
2016, 9801, 98010P.
[8] Roundy, S., Wright, P. K., & Rabaey, J. (2003). A study of low level vibrations as a power source for wireless sensor nodes. Computer Communications, 26(11), 1131–1144.
[9] Nakamura, K., & Shimizu, H. (1989). Ferroelectrics Hysteresis-free piezoelectric actuators using $LiNbO_3$ plates with a ferroelectric inversion layer. Ferroelectrics, 93, 211–216.
[10] Nakamura, K., Ando, H., & Shimizu, H. (1987). Bending vibrator consisting of a $LiNbO_3$ plate with a ferroelectric inversion layer. Japanese Journal of Applied Physics, 26, 198–200.
[11] Clementi, G., Ouhabaz, M., Margueron, S., Suarez, M. A., Bassignot, F., Gauthier-Manuel, L., Belharet, D., Dulmet, B., Bartasyte, A. (2021). Highly coupled and low frequency vibrational energy harvester using lithium niobate on silicon. Applied Physics Letters, 119(1), 013904.
[12] Machado, L. Q., Yurchenko, D., Wang, J., Clementi, G., Margueron, S., Bartasyte, A. (2021). Multi-dimensional constrained energy optimization of a piezoelectric harvester for E-gadgets. iScience, 24 (7), 102749.
[13] Clementi, G., Lombardi, G., Margueron, S., Suarez, M. A., Lebrasseur, E., Ballandras, S., Imbaud, J., Lardet-Vieudrin, F., Gauthier-Manuel, L., Dulmet, B., Lallart, M., Bartasyte, A. (2021). $LiNbO_3$ films – A

low-cost alternative lead-free piezoelectric material for vibrational energy harvesters. Mechanical Systems and Signal Processing, 149, 107171.
[14] Panayanthatta, N., Clementi, G., Ouhabaz, M., Costanza, M., Margueron, S., Bartasyte, A., Basrour, S., Bano, E., Montes, L., Dehollain, C., La Rosa, R. (2021). A Self-Powered and Battery-Free Vibrational Energy to Time Converter for Wireless Vibration Monitoring. Sensors, 21, 7503.
[15] Vidal, J. V., Turutin, A. V., Kubasov, I. V., Kislyuk, A. M., Malinkovich, M. D., Parkhomenko, Y. N., Kobeleva, S.P., Pakhomov, O. V., Sobolev, N. A., Kholkin, A. L. (2019). Low-Frequency Vibration Energy Harvesting with Bidomain LiNbO3 Single Crystals. IEEE Transactions on Ultrasonics, Ferroelectrics, and Frequency Control, 66 (9), 1480–1487.
[16] Shur, V. Y., Baturin, I. S., Mingaliev, E. A., Zorikhin, D. V., Udalov, A. R., & Greshnyakov, E. D. (2015). Hysteresis-free high-temperature precise bimorph actuators produced by direct bonding of lithium niobate wafers. Applied Physics Letters, 106 (5), 053116.
[17] Williams, C. B., & Yates, R. B. (1996). Analysis of a micro-electric generator for microsystems. Sensors and Actuators, A: Physical, 52 (1–3), 8–11.
[18] Roundy, S., & Wright, P. K. (2004). A piezoelectric vibration based generator for wireless electronics. Smart Materials and Structures, 13(5), 1131–1142.
[19]Mason, Warren P.(1948). Electromechanical Transducers and Wave Filters, *Van Nostrand Reinhold Inc.*,
[20] Tiersten, H.F. (1969). Linear Piezoelectric Plate Vibrations (Plenum, New York).
[21] Tanaka, H. (1994) Generalized basic Equations for bending motions of piezoelectric bars formulated from Hamilton's principle. The Journal of the Acoustical Society of America, 95(4), 1768–1772.
[22] DuToit, N. E., Wardle, B. L., & Kim, S. G. (2005). Design considerations for MEMS-scale piezoelectric mechanical vibration energy harvesters. Integrated Ferroelectrics, 71, 121–160.
[23] He, X., Li, D., Zhou, H., Hui, X., & Mu, X. (2021). Theoretical and experimental studies on MEMS variable cross-section cantilever beam based piezoelectric vibration energy harvester. Micromachines, 12 (7), 772.
[24] Gibus, D., Gasnier, P., Morel, A., Formosa, F., Charleux, L., Boisseau, S., Pillonnet, G., Berlitz, C. A., Quelen, A., Badel, A. (2020). Strongly coupled piezoelectric cantilevers for broadband vibration energy harvesting. Applied Energy, 277.
[25] Lefeuvre, E., Badel, A., Richard, C., Petit, L., & Guyomar, D. (2006). A comparison between several vibration-powered piezoelectric generators for standalone systems. Sensors and Actuators, A: Physical, 126 (2), 405–416.
[26] Badel, A., Lagache, M., Guyomar, D., Lefeuvre, E., & Richard, C. (2007). Finite element and simple lumped modeling for flexural nonlinear semi-passive damping. Journal of Intelligent Material Systems and Structures, 18 (7), 727–742.
[27] Erturk, A., & Inman, D. J. (2008). Issues in mathematical modeling of piezoelectric energy harvesters. Smart Materials and Structures, 17 (6), 065016.
[28] Erturk, A., & Inman, D. J. (2008). On Mechanical Modeling of Cantilevered Piezoelectric Vibration Energy Harvesters. Journal of Intelligent Material Systems and Structures, 19 (11), 1311–1325.
[29] IEEE Standard on Piezoelectricity: An American National Standard. ANSI/IEEE Std 176-1987 (1988).
[30] Warner, A. W., Onoe, M., & Coquin, G. A. (1968). Determination of Elastic and Piezoelectric Constants for Crystals. The Journal of the Acoustical Society of AmericaAcoustical Society of America, 930, 1223–1231.
[31] Kovacs, G., Anhorn, M., Engan, H. E., Visintini, G., & Ruppel, C. C. W. (1990). Improved material constants for $LiNbO_3$ and $LiTaO_3$. Ultrasonics Symposium Proceedings, 1, 435–438.
[32] Fan, Y., Ghayesh, M. H. & Lu, Tien-Fu (2022). High-efficient internal resonance energy harvesting: Modelling and experimental study. Mechanical Systems and Signal Processing, 180, 109402
[33] Fan, Y., Ghayesh, M. H., Lu, T.-F., Amabili, M. (2022). Design, development, and theoretical and experimental tests of a nonlinear energy harvester via piezoelectric arrays and motion limiters.

International Journal of Non-Linear Mechanics, 142, 103974
[34] Mallick, D., Roy S., (2015). "Bidirectional electrical tuning of FR4 based electromagnetic energy harvesters", Sens. Actuators A-Phys., 226 154.

[35] Bartasyte, A., Clementi, G., Micard, Q., Labbaveettil, I., Sousa Lopes Moreira, A., Boujnah, S., Ouhabaz, M., Verma, A., Ichangi, A. Malandrino, G., Mathur, S., Dulmet, B., Margueron, S. (2023). “Material strategies to enhance the performance of piezoelectric energy harvesters based on lead-free materials”, J. Micromech. Microeng. 33, 053001.